We are IntechOpen, the world's leading publisher of Open Access books
Built by scientists, for scientists

6,900
Open access books available

185,000
International authors and editors

200M
Downloads

154
Countries delivered to

Our authors are among the

TOP 1%
most cited scientists

12.2%
Contributors from top 500 universities

CLARIVATE ANALYTICS
BOOK CITATION INDEX
INDEXED

WEB OF SCIENCE™

Selection of our books indexed in the Book Citation Index
in Web of Science™ Core Collection (BKCI)

Interested in publishing with us?
Contact book.department@intechopen.com

Propagation Buckling of Subsea Pipelines and Pipe-in-Pipe Systems

Hassan Karampour and Mahmoud Alrsai

Abstract

This chapter investigates buckle propagation of subsea single-walled pipeline and pipe-in-pipe (PIP) systems under hydrostatic pressure, using 2D analytical solutions, hyperbaric chamber tests and 3D FE analyses. Experimental results are presented using hyperbaric chamber tests, and are compared with a modified analytical solution and with numerical results using finite element analysis for single-walled pipelines and PIPs. The experimental investigation is conducted using commercial aluminum tubes with diameter-to-thickness (D/t) ratio in the range 20–48. The comparison indicates that the modified analytical expression presented in this work provides a more accurate lower bound estimate of the propagation buckling pressure of PIPs compared to the existing equations, especially for higher D_o/t_o ratios. A 3D FE model is developed and is validated against the experimental results of the propagation bucking. A parametric FE study is carried out and empirical expressions are provided for buckle propagation pressures of PIPs with (D_o/t_o) ratio in the range 15–25. Moreover, empirical expressions are proposed for the collapse pressure of the inner pipe (P_{ci}), the proposed empirical equation for P_{ci}, is shown to agree well with the experimental results of the tested PIPs.

Keywords: collapse pressure, external pressure, offshore pipelines, pipe-in-pipe, propagation buckling

1. Propagation buckling of single pipe

1.1 Introduction

Deep and ultra-deep water pipelines are vulnerable to propagation buckling due to the high external pressures. The pipeline may collapse due to the local dents, imperfections and ovalizations in the pipe-wall. This collapse will change the cross-section of the pipeline from a circular shape into a dog-bone or even flat shape. The buckle may then propagate along the pipeline and cause the pipeline to be shut down. A typical propagation buckle scenario is shown in **Figure 1**, which is triggered by impact on the pipeline from an anchor dropped from a passing vessel.

Different stages of the buckle are shown in **Figure 1** in terms of the external pressure versus change in volume of the pipe. The dent caused by the impact can initiate the buckle due to high external pressure. The elastic buckling is followed by a plastic collapse and change in the cross-section of the tube from circular to oval
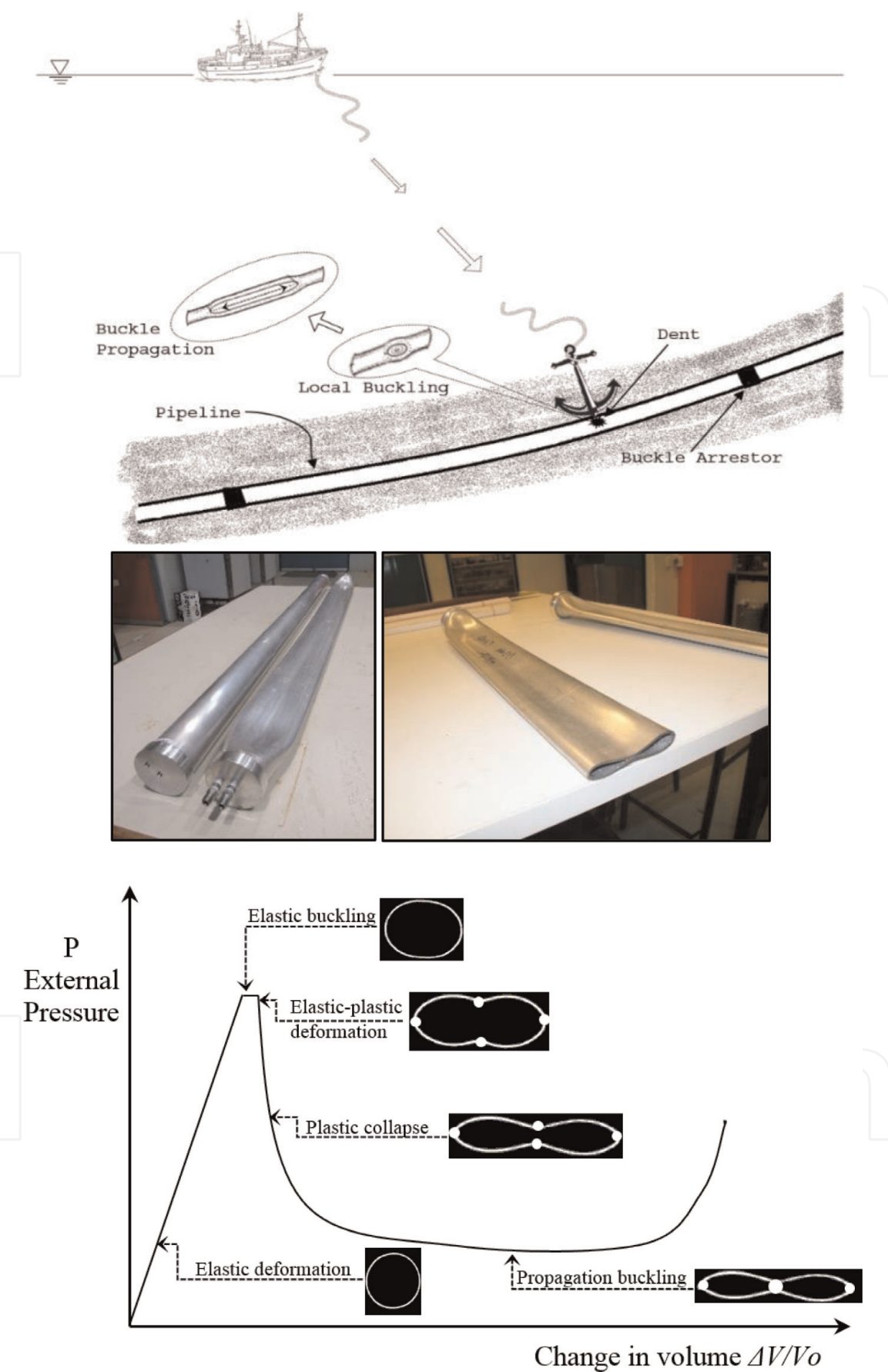
Figure 1.
Buckle propagation scenario [1].

and finally a dog-bone shape. If the pressure is maintained, the buckle will propagate quickly along the length of the pipe. Offshore pipelines normally experience high service external pressure; therefore the buckle will propagate through the

length, forcing the flow line to be shut. The lowest pressure that maintains propagation is known as the propagation pressure, and is much smaller than the collapse pressure. To account for the difference between the collapse and the propagation pressures in design, a thick-walled pipeline is required [1, 2].

As shown in **Figure 1**, the propagation pressure is much less than initiation pressure (peak pressure in **Figure 1**). The initiation pressure is significantly affected by the size of the local dent. Local dents may also occur during the installation period. The most common types of offshore pipeline installation are S-lay method, J-lay method, Reel-lay method and Towing method. A combination of bending and external pressure happens in the sag bend length of the pipe. Normally high tension is applied to the pipe to maintain its stiffness during installation. If for any reason this tension is released, high bending in the sag bend region may cause local buckling which may be followed by propagation buckling. Apart from the foretold loading sources, manufacturing imperfections in pipe such as non-uniform thickness, varying elastic modulus, local ovalization, and also erosion and corrosion may cause local buckling in pipelines.

Many researchers have investigated various aspects of this problem since it was first presented by Mesloh et al. [3] and Palmer and Martin [4]. Most notably is the extensive work of Kyriakides [5, 6], Kamalarasa [7] and Albermani et al. [2]. Recent books by Kyriakides [1] and Palmer and King [8] provide comprehensive review of this problem and the associated literature. The work done by Xue et al. [9] investigates the effect of corrosion in the propagation buckling of subsea pipelines. Buckle arrestors [1, 18], pipe-in-pipe system [10–14], sandwich pipe system [15] and ring-stiffened pipelines [16], are used to confine the propagation buckling in subsea pipelines.

As stated before, a local dent or ovalization in the pipe wall can cause a local collapse as in the pipe-wall. It is well-known that the collapse pressure of a 2D arch (similar to a single pipeline (P_{cr})), under lateral pressure can be approximated by [17]:

$$P_{cr} = \frac{E}{4(1 - \nu^2)} \left(\frac{t}{r}\right)^3 \tag{1}$$

where E is the modulus of elasticity, ν is the Poisson's ratio, t is the pipe wall thickness and r is the mean radius of pipe. As shown in **Figure 1** prior to the collapse pressure no significant change in cross section of pipe is observed. Note that for sake of clarity the slope of line ending to collapse pressure in **Figure 1** is exaggerated. During the propagation buckling the pipe endures substantial change in its shape.

1.2 Analytical solution of propagation pressure of single pipe

A typical buckle propagation response is characterized by the pressure at which the snap-through takes place (the initiation pressure P_I) and the pressure that maintains propagation (the propagation pressure P_p) which is a small fraction of P_I.

Palmer and Martin [4] suggested a 2D approximation for propagation buckling of subsea pipelines Eq. (2). Their solution is based on a 2D ring collapse (plane strain) mechanism, and accounts for the circumferential bending effect of the pipe wall (see **Figure 2**). The Palmer and Martin (PM) solution underestimates the propagation pressure when compared to experimental results. This difference increases as D/t decreases. The propagation pressure from the PM solution, P_{PM}, is given by:

$$P_{PM} = \frac{\pi}{4} \sigma_y \left(\frac{t}{r}\right)^2 \tag{2}$$

for a pipe with radius, r, wall thickness, t, and material yield stress, σ_y. Based on experimental observations from hyperbaric chamber tests, the top and bottom hinges in **Figure 2a** move towards each other while the left and right hinges move laterally away from each other. This deformation continues until touchdown (**Figure 2b**), the lateral movement seizes and flattening of the resulting four arch segments commence (**Figure 2c**).

Accordingly, a modification to the lower bound PM solution is proposed [2], by accounting for the circumferential membrane as well as flexural effects in the pipe wall

$$W_{ex} = (W_{in})_f + (W_{in})_m \tag{3}$$

where W_{ex} is the external work done by the net hydrostatic pressure and W_{in} is the internal work due to circumferential flexure, f, and membrane, m, effects. The initially circular cross section of the pipe (**Figure 2a**) will deform into a dog-bone (**Figure 2b**) and eventually into a nearly flat segment. Accordingly, (Eq. (3)) can be written as:

$$p(\Delta A) = 3\pi m_p + (pr)(\Delta l) \tag{4}$$

where ΔA is the change in the cross section area, Δl is the change in the circumferential length and m_p is the plastic moment, these are given by:

$$\Delta A = \pi r^2 \tag{5}$$
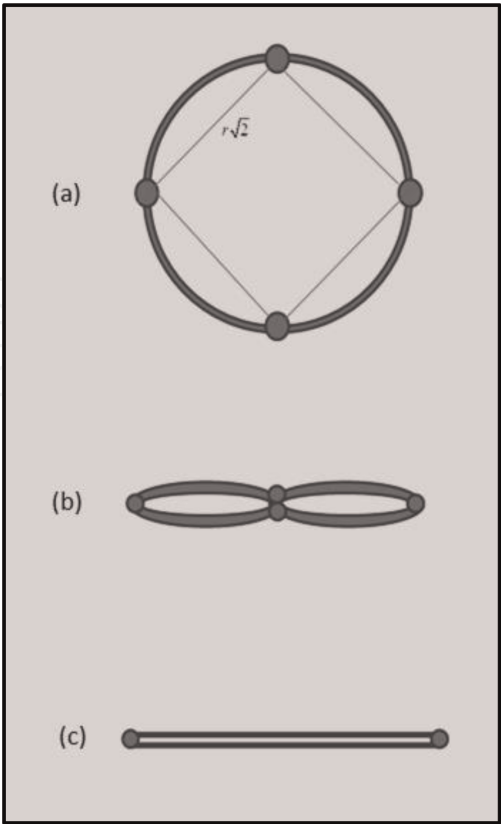
Figure 2.
A schematic of 2D deformation stages in propagation buckling of single pipe; (a) the initial circular cross section of the single pipe; (b) dog-bone deformed shape; (c) flat segment of the pipe.

$$\Delta l = 0.626r \tag{6}$$

$$m_p = \sigma_y \frac{t^2}{4} \tag{7}$$

Substituting Eqs. (5)–(7) into (4), the propagation pressure, $\widetilde{p}$, is obtained as:

$$\widetilde{p} = \frac{3}{2.515}\left[\frac{\pi}{4}\sigma_y\left(\frac{t}{r}\right)^2\right] = 1.193 p_{PM} \tag{8}$$

Experimental observations confirm that the propagation pressure predicted by (Eq. (8)) is 19% higher than the PM prediction Eq. (2), regardless of t/r ratio. However, it should be noted, that by adopting plane strain conditions, the tensile coupon yield stress can be augmented by a factor of $(2/\sqrt{3})$ in (Eq. (8)) which results in an additional 15% increase in $\widetilde{p}$.

1.3 Experiments on propagation buckling of single-walled pipelines

A stiff 4 m long hyperbaric chamber rated for 20 MPa (2000 m water depth) internal pressure was used for testing (**Figure 3a**). Three meter long aluminum pipes were used in the hyperbaric chamber tests [2]. Ovalization measurements along the pipe samples before testing were carried out that gave an average ovalization ratio Ω (Eq. (9)) around 0.46–0.67%
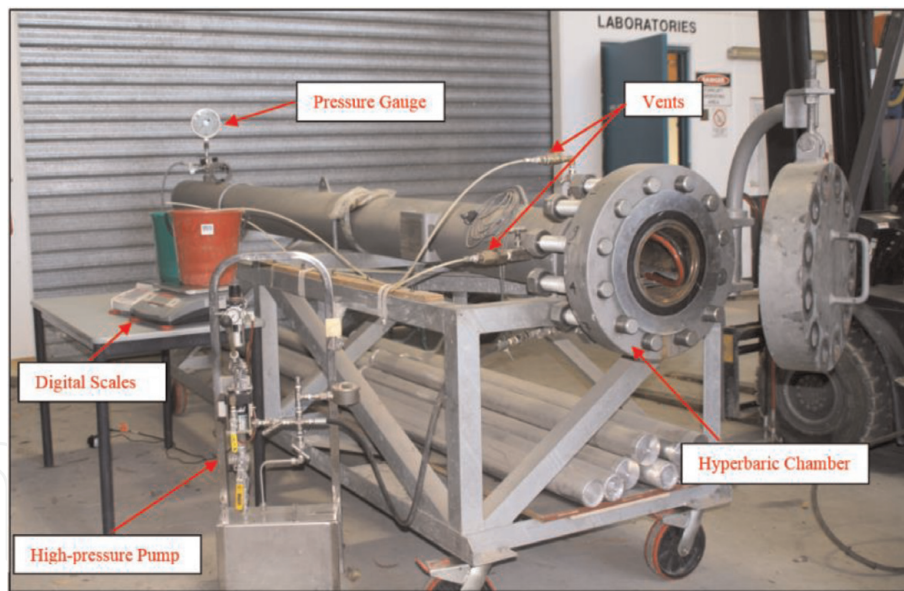
(a)

(b)   (c)

Figure 3.
The experimental set-up: (a) the hyperbaric chamber, high-pressure pump, scales, pressure gauge and vents, (b) pipes and fittings, (c) failed pipes tested in the hyperbaric chamber.

$$\Omega_0 = \frac{D_{\max} - D_{\min}}{D_{\max} + D_{\min}} \tag{9}$$

where D_{max} and D_{min} are the maximum and minimum measured outer diameters along the pipe length.

The hyperbaric chamber test procedure is as follows. Thick discs are welded at both ends of 3 m pipeline. The pipeline is then filled with water and inserted inside the chamber (**Figure 3b**). The bolts at the chamber lid are tightened using a pneumatic torque wrench and the chamber is sealed. Using a control-volume analogy, the water inside the chamber is pressurized at a slow rate, using a hand pump. When the pressure reaches the initiation pressure P_I of the pipeline, a section along the pipe sample collapses. This leads to a substantial drop in chamber pressure and is followed by water flowing from within the pipe sample through vent. Then, the chamber pressure is stabilized at the propagation pressure, P_p, with the buckle longitudinally propagating along the pipe sample accompanied by uniform water flow from the vent. The failed samples are sown in **Figure 3c**.

The average pressures of the 19 pipes tested in the hyperbaric chamber are represented in **Table 1**. A typical pressure-volume change response obtained from the hyperbaric chamber tests is shown in **Figure 4**. In **Figure 4**, the pressure inside the chamber is normalized by the propagation pressure, P_{PM}, and the change in the pipe volume ΔV is normalized by the initial volume of the pipe, V. As stated before, the buckle initiation pressure, P_I, is sensitive to imperfections (such as a dent in the pipe wall). However, the buckle propagation pressure, P_p, is not affected by the imperfection.

The analytical, experimental and numerical pressures are compared in **Table 2**. The ratio of propagation pressure from the hyperbaric chamber tests P_P to the

Sample/material		D/t	Coupon tests			Analytical (MPa)		Hyperbaric chamber (MPa)			
ID	Al-6060		σ_Y (MPa)	E/σ_Y	$E'/E(\%)$	P_{PM} Eq. (2)	$\widetilde{P}$ Eq. (8)	Experiment		Finite element	
								P_I	P_P	P_{IFE}	P_{PFE}
D50	T591	25	122	440	1.5	0.778	0.93	6.42	1.6	5.12	1.1
D60	T4	20	81	716	1.9	1.011	1.21	8.24	2.3	8.15	1.6
D76	T5	47.5	156	367	0.4	0.205	0.245	1.32	0.35	1.07	0.3

Table 1.
Summary of experimental, analytical and numerical results.
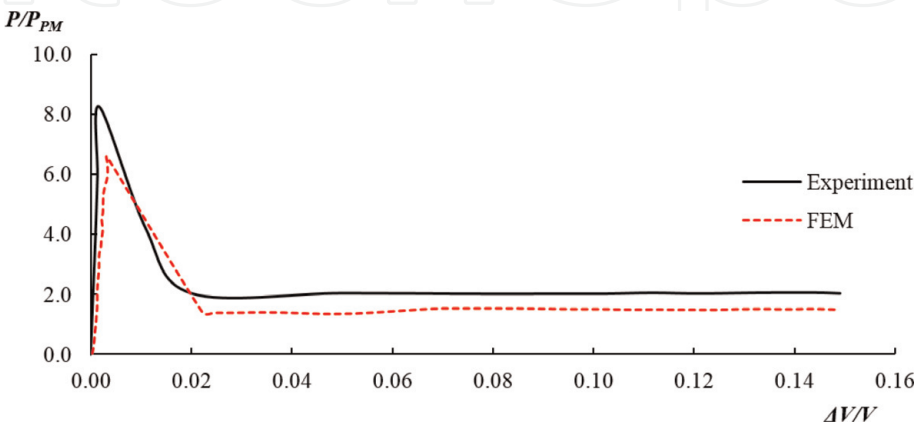
Figure 4.
Normalized pressure-volume response (experimental and numerical results) for D50.

Sample	D/t	Hyperbaric chamber		Finite element	
		$P_P/\tilde{P}$	P_I/P_P	P_I/P_{IFE}	P_P/P_{PFE}
D50	25	1.720	4.01	1.253	1.453
D60	20	1.900	3.58	1.011	1.437
D76	47.5	1.428	3.77	1.234	1.167

Table 2.
Comparison of experimental, analytical and numerical results.

modified analytical solution $\tilde{p}$ (Eq. (8)) vary from 1.428 to 1.9 depending on D/t ratio. Mesloh et al. [19] suggested similar relations. The ratio of P_I/P_P from the hyperbaric chamber tests is also shown in **Table 2** and varies from 3.5 to 4.0. The results represented in **Table 2** highlight the susceptibility of deep and ultra-deep subsea pipelines to propagation buckling. To confine the buckle propagation, external ring stiffeners are exploited intermittently on the pipeline. These buckle arrestors can only confine the pressure between two stiffeners.

1.4 Finite element study on propagation buckling of single-walled pipelines

FE models were created in ANSYS [20] to investigate the response of the pipe to propagation buckling. Thin 4-noded shell elements (181) were used to model the pipe. SHELL181 is suitable for analyzing thin to moderately-thick shell structures. It is a four-noded element with six degrees of freedom at each node: translations in the x, y, and z directions, and rotations about the x, y, and z axes. Hydrostatic pressure can be applied as surface loads on corresponding surface. Pipe wall thickness is defined using section data command. A convergence study was performed and five integration points was found to be adequate for propagation buckling of cylindrical pipes. Frictionless contact and target elements (ANSYS elements 174 and 170) are used to define the contact between the inner surfaces of the pipe wall. These elements are created on the surface of the existing shell elements using ESURF command. The 3D contact surface elements CONTA174 are associated with the 3D target segment elements TARGE170 via a shared real constant set. Contact stiffness can be controlled by normal penalty stiffness factors and tangent penalty stiffness factor. Normal penalty stiffness factor of 0.1 was selected based on a convergence study performed that ensures both real contact behavior and reasonable computational time. Tangent stiffness factor appeared not to affect the results significantly.

A von-Mises elastoplastic material definition with isotropic hardening was adopted based on material properties shown in **Table 1**. Total of 40 shell-181 elements in circumference were utilized for modeling the pipe. Local ovalizations were introduced to FE model by applying external pressures symmetrically on 8 elements on top of the pipe along a length equal to diameter of the pipe. Geometry is then updated using UPGEOM command and nonlinear geometric and material analysis is carried out. The FE model is 3 m long and is restrained against translation at all nodes at both ends.

The initiation and propagation pressures obtained from FE analysis (P_{IFE} and P_{PFE} respectively) are summarized in **Table 1** and are in reasonable agreement with the experimental results from the hyperbaric chamber. Unlike buckle initiation pressure (P_I), buckle propagation pressure (P_P) is independent of curvature or ovalization of pipe. Palmer and Martin prediction P_{PM} estimates a lower bound for propagation pressure. The FE predictions of initiation and propagation pressures on
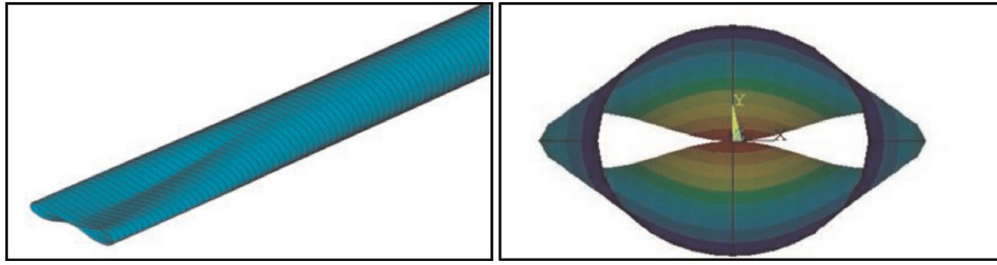
Figure 5.
FE model of 3 m long D50 showing the onset of propagation buckling.

average represent 87 and 74%, respectively, of the experimental results. A typical FE result for D50 pipe is shown in **Figures 4** and **5**.

2. Propagation buckling of pipe-in-pipe systems

2.1 Introduction

Pipe-in Pipe (PIP) systems are extensively being used in the design of high pressure and high temperature (HP/HT) flowlines due to their outstanding thermal insulation. A typical PIP system consists of concentric inner and outer pipes, bulk heads and centralizers. The inner pipe (flowline) conveys the production fluids and the outer pipe (carrier pipe) protects the system from external pressure and mechanical damage. The two pipes are isolated by centralizers at joints and connected through bulkheads at the ends of the pipeline. The annulus (space between the tubes) is either empty or filled with non-structural insulation material such as foam or water [21].

PIP systems are normally divided into two categories, namely, compliant and non-compliant systems. In a compliant system, the inner pipe and the carrier pipe are attached at close intervals; whereas both inner and carrier pipes are only connected through bulkheads at discrete locations in a non-compliant system. The relative movement between the inner and outer pipes is arrested in a compliant system while the two pipes can move relative to each other in a non-compliant system. PIPs are exploited in subsea developments, where the carrier pipe is designed to resist high hydrostatic pressures (water depths up to 3000 m) and the inner pipe is designed to transmit hydrocarbons at temperatures as high as 180°C [22]. The HP/HT flow can cause global upheaval [23] or lateral buckling [24] in the system. Furthermore, the high hydrostatic pressure may trigger a local collapse, such as propagation buckling or buckle interaction [13–14, 25–29, 33], in the carrier (outer) pipe. Structural integrity of the PIP system under external pressure is an issue of concern, because the collapse of the carrier pipe may result in collapse of the inner pipe.

Despite the extensive investigations performed on integrity of single pipelines, to date, instabilities of PIPs have only been marginally addressed. Kyriakides [10] conducted a thorough experimental study on propagation buckling of steel PIPs with two-inch diameter carrier tubes with D_o/t_o values of 24.1, 21.1 and 16.7 and inner pipes of various D_i/t_i ratios ranging between 15 and 37. Kyriakides [10] observed two dominant modes of buckling. In the first mode the local collapse of the outer pipe led to simultaneous collapse of the inner pipe, whereas in the second mode the carrier pipe collapsed without affecting the inner pipe. Based on the experimental study and 3D finite element analyses, Kyriakides and Vogler [11] suggested an empirical formula for buckle propagation pressure of PIP, P_{p2}. Gong

and Li [12] carried out a finite element study of propagation buckling of PIPs with carrier pipes having D_o/t_o values of 25, 20 and 15 and inner tubes having D_i/t_i of 15 and 20. Although both studies [11, 12] covered similar D_o/t_o range of the carrier pipe, two different empirical expressions were suggested.

2.2 Analytical solution of propagation pressure of pipe-in-pipe systems

Numerous analytical solutions have been suggested to estimate the propagation pressure of a single pipe. Unlike propagation pressure, the initiation pressure is very sensitive to initial imperfection such as local dents or ovalizations. The propagation pressure is related to plastic properties of the pipe and is only a fraction of the buckle initiation pressure. Both buckle initiation pressure and buckle propagation pressure are related to the diameter to wall-thickness ratio of the pipe, however previous studies suggest that there is no evident relationship between the two [2, 3]. The simplest propagation pressure model was established by Palmer and Martin [4], which only considered the initial and final configurations of the cross-section of the pipe. **Figure 6** shows the four plastic hinges developed in the pipe at different stages of propagation buckling on subsea pipelines and pipe-in-pipe systems.

By adopting plane strain analogy, Kyriakides and Vogler [11] proposed the following expression for the propagation pressure of the PIP system. Their formulation accounts for development of four plastic hinges in each of the carrier and the inner pipes (**Figure 6d-f**).

$$\hat{P}_{p2} = \frac{2\pi}{\sqrt{3}}\sigma_{Yo}\left(\frac{t_o}{D_o}\right)^2\left[1 + \frac{\sigma_{Yi}}{\sigma_{Yo}}\left(\frac{t_i}{t_o}\right)^2\right] \qquad (10)$$

where subscripts o and i denote the outer pipe and inner pipe, respectively.

The analytical lower bound solution to propagation buckling of a single pipe given by (Eq. (8)), can be extended to the pipe-in-pipe systems by accounting for the membrane and flexural effects of the outer and the inner pipes:

$$W_{ex} = W_{in(f)} + W_{in(m)} \qquad (11)$$
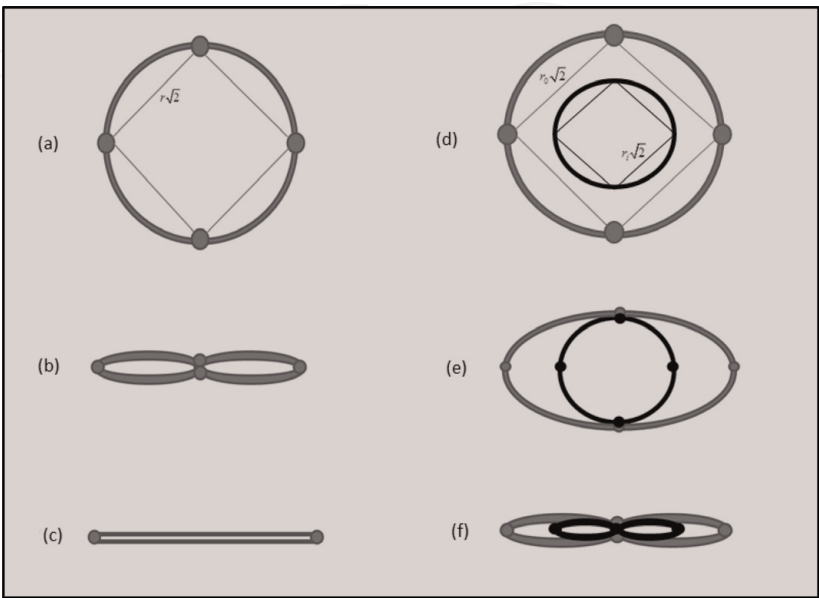
Figure 6.
A schematic of deformation stages in propagation buckling of a single pipe (stages a–c) and a pipe-in-pipe system (stages d–f).

where W_{ex} is the external work done by the hydrostatic pressure and W_{in} is the internal work due to the circumferential flexure, f and membrane effects, m. Based on the experimental observations from the hyperbaric chamber, the initially circular cross-section of the outer pipe (**Figure 6d**) has found to deform into the shape shown in (**Figure 6e**). Further increase in the external pressure causes the pipe-in-pipe system to eventually deform into the dog-bone shape (**Figure 6f**). Thus (Eq. (11)) can be written as:

$$\overline{P}_{p2}(\Delta A) = 3\pi(m_{po} + m_{pi}) + \overline{P}_{p2}(r_o.\Delta l_o + r_i.\Delta l_i) \tag{12}$$

where ΔA is the change in the cross-section area, Δl is the change in the circumferential length and mp is the plastic moment. These are given by:

$$\Delta A = \pi r_o^2 \tag{13}$$

$$\Delta l_o = \left(2\pi - 4\sqrt{2}\right)r_0; \quad \Delta l_i = \left(2\pi - 4\sqrt{2}\right)r_i \tag{14}$$

$$m_{po} = \sigma_{Yo}\frac{t_o^2}{4}; \quad m_{pi} = \sigma_{Yi}\frac{t_i^2}{4} \tag{15}$$

where the subscript "o" denotes the outer pipe, and "i" represents the inner pipe. Substituting Eqs. (13)–(15) into (12), the propagation pressure, $\overline{P}_{p2}$, of the PIP system is obtained as:

$$\overline{P}_{p2} = \left[\frac{3\pi\sigma_{Yo}}{2.515}\left(\frac{t_o}{D_o}^2\right)\right]\left[1 + \frac{\sigma_{Yi}}{\sigma_{Yo}}\left(\frac{t_i}{t_o}\right)^2\right]\left[\frac{1}{1 - (D_i/2D_o)^2}\right] \tag{16}$$

When $D_i = t_i = 0$, Eq. (16) yields the propagation pressure of a single pipe given by Eq. (8). Unlike Eq. (10), Eq. (16) accounts for the effect of D_i/D_o as well as that of t_i/t_o and σ_{Yi}/σ_{Yo}.

2.3 Experiments on propagation buckling of pipe-in-pipe system

The experimental protocol is comprised of end-sealing concentric PIP systems with parameters shown in **Table 3** and a length of 1.6 m ($L/D > 20$), being pressurized inside the hyperbaric chamber depicted in **Figure 3a**. The chamber has an inner-diameter of 173 mm and a length of 4 m and is rated for working pressure of 20 MPa (2000 m water depth). The intact PIP was sealed at both ends by gluing on thick aluminum discs ensuring that the inner was completely sealed from the outer pipe. Two valves were connected to each end of the PIP, one on the carrier pipe and

ID	Carrier pipe	Inner pipe	D_o/t_o	D_i/t_i	D_i/D_o	t_i/t_o	E (MPa)	$\frac{E'}{E}$ (%)	σ_{Yo} (MPa)	$\frac{\sigma_{Yi}}{\sigma_{Yo}}$
PIP-1	OD = 80, t = 2	OD = 40, t = 1.6	40.0	25.0	0.50	0.80	69,000	1.01	169	0.93
PIP-2	OD = 60, t = 2	OD = 40, t = 1.6	30.0	25.0	0.75	0.80	69,000	0.97	139	1.12
PIP-3	OD = 80, t = 3	OD = 40, t = 1.6	26.7	25.0	0.50	0.53	69,000	1.02	209	0.75

Note: All dimensions are in millimeters; OD = outer diameter; t = thickness.

Table 3.
Properties of PIPs.
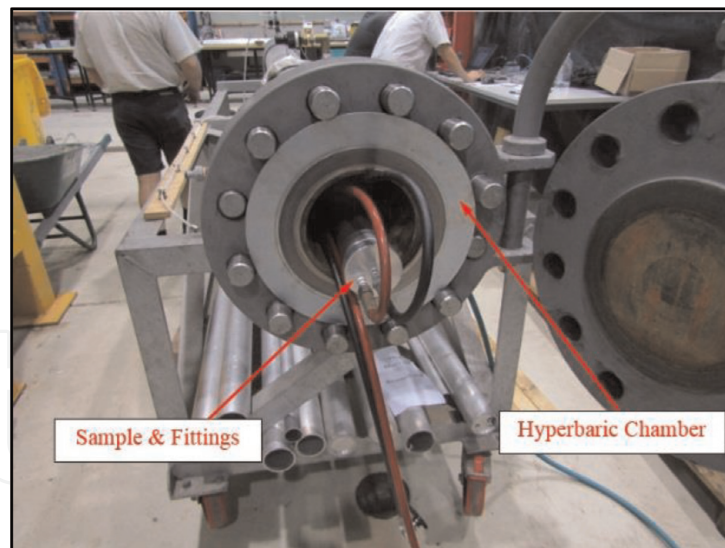
Figure 7.
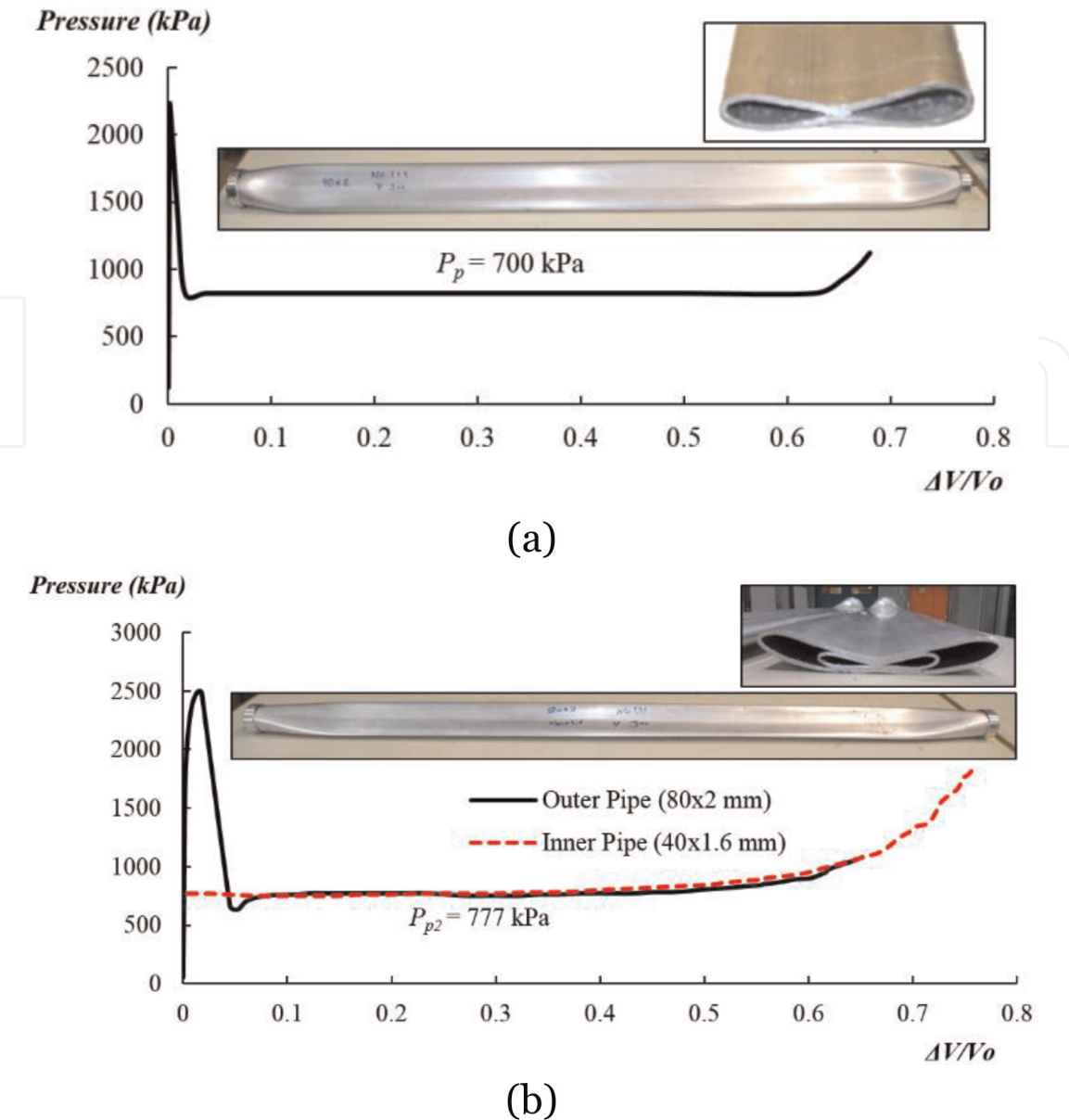*The PIP sample inside the hyperbaric chamber and fittings.*

the other on the inner pipe. One valve was used for bleeding the pipe while filling it with water. The second valve was utilized to vent the carrier and inner pipes, as well as to collect water from the inner pipe and the cavity between the inner and outer pipes during the buckle propagation (through the red and black hoses shown in **Figure 7**). A volume-controlled pressurization with a high pressure pump (shown in **Figure 3a**) was used and the pressure was increased until collapse of the system due to external pressure occurred under quasi-static steady-state conditions. By maintaining a low rate of pumping, the chamber pressure was stabilized at propagation pressure P_{p2}, with buckle longitudinally propagating along the PIP sample accompanied by water flow from the vents. The change in volume of the system (ΔV) during the test was calculated by measuring the weight of water being discharged from the inner pipe and the cavity between the pipes separately using digital weighing scales shown in **Figure 3a**. Control tests using a single pipe (outer pipe) were conducted first.

Figures 8–10 present the experimental results of the buckle propagation response of PIPs. The pressure inside the chamber is plotted against the normalized change in volume of the carrier pipe (60 × 2 mm) of PIP-2 in **Figure 8a**. The chamber is gradually pressurized until the initiation pressure P_I is reached at which a section of the pipe collapses resulting in a drastic drop in the chamber's pressure. The pressure is then maintained at the propagation pressure P_p with the dog-bone buckle shape longitudinally propagating along the length of the pipe. The buckle propagation response of the PIP-2 system is shown in **Figure 8b**. The change in pressure of the system is plotted against the normalized change in volume of the inner pipe (40 × 1.6 mm) and the outer pipe (60 × 2 mm) (the space between the two pipes). Buckle is initiated first (P_{I2}) on the outer pipe, then the energy is released through ovalization of the outer pipe, until the outer pipe touches the inner pipe. Buckle initiation pressures P_I and PI_2 have been shown to be closely related to geometric imperfections in shapes of dents or ovality of the outer pipe [25, 30]. Since the main focus of the present study is only on the buckle propagation pressures, the parameters affecting the buckle initiation pressure are not discussed herein. Following the contact between the carrier pipe and the inner pipes of PIP-2, the inner pipe collapses and the buckle propagates longitudinally as long as the pressure is maintained at P_{p2}. When the stiff end-caps fall within the vicinity of the buckle transition zone, a higher pressure is required to perpetuate the buckle which corresponds to the stiffening part of PIP-2 response shown in **Figure 8b**.
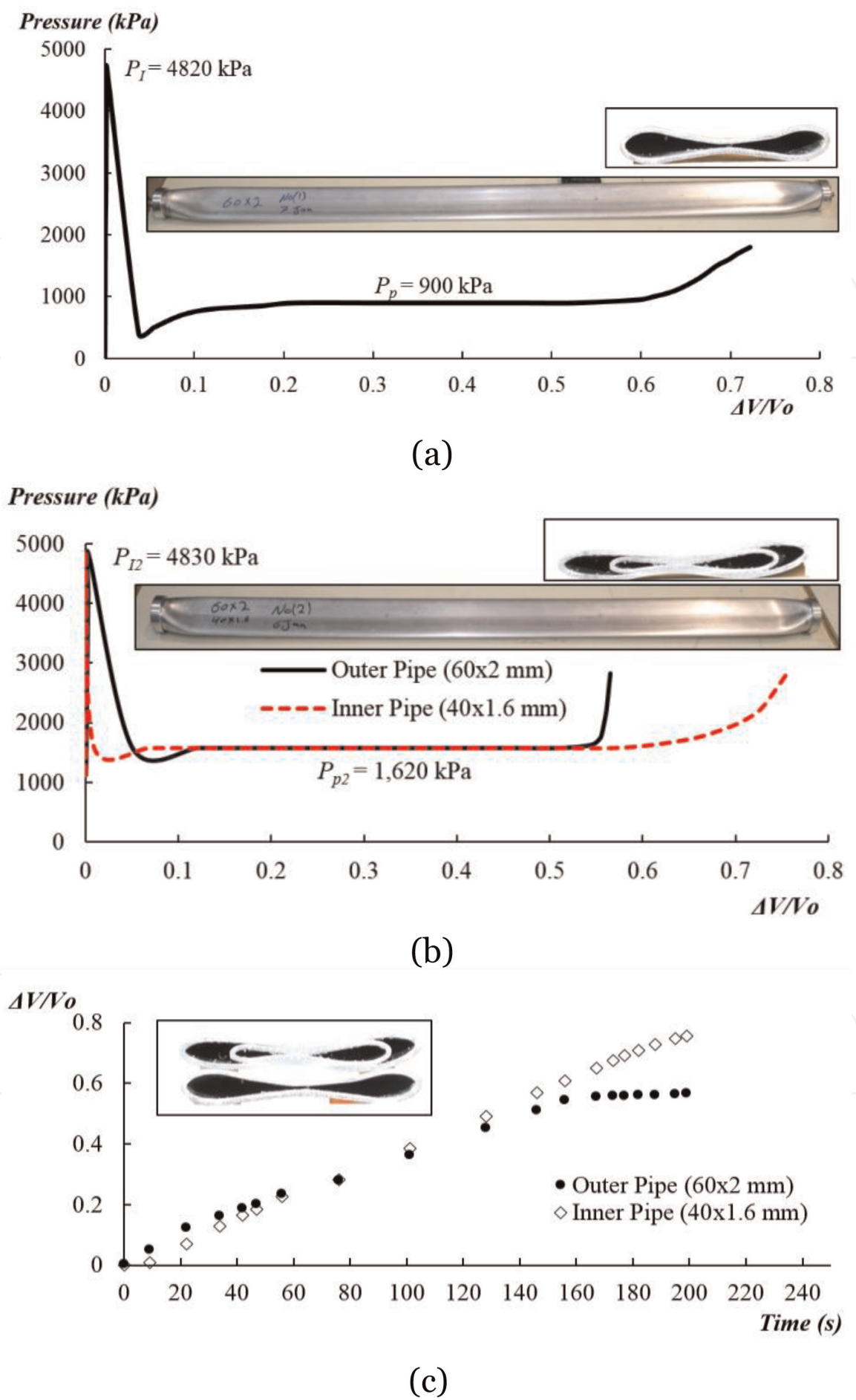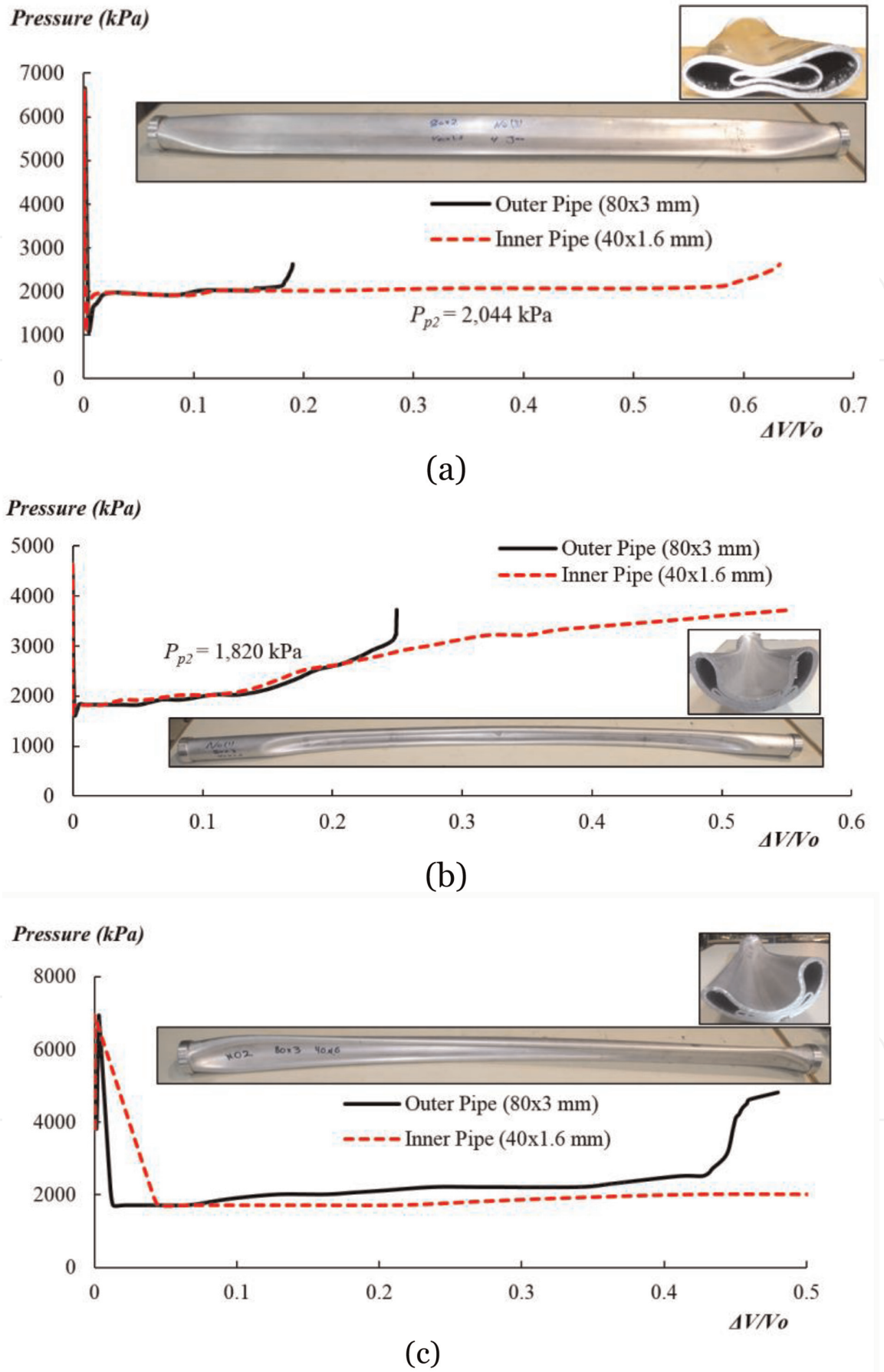
Figure 8.
Buckle propagation response inside the hyperbaric chamber: (a) pressure versus normalized change of volume of the 60 × 2 mm carrier pipe, (b) pressure versus normalized change of volume of PIP-2 and (c) normalized volume versus time of PIP-2.

(a)

(b)

Figure 9.
Buckle propagation response inside the hyperbaric chamber: (a) pressure versus normalized change of volume of the 80 × 2 mm carrier pipe, (b) pressure versus normalized change of volume of PIP-1.

A dog-bone buckle shape similar to that observed in buckle propagation of the carrier pipe (**Figure 8a**) was detected in the PIP-2 chamber test (**Figure 8b**). Change in volume of the outer and inner pipes are plotted against the test time in **Figure 8c**. The time-history shows a higher initial discharge from the outer pipe than the inner pipe. However, after the outer pipe touches the inner pipe at $\Delta V/V_o = 0.1$ (shown in **Figure 8b**), discharge from the inner pipe is triggered and at $\Delta V/V_o > 0.2$ (shown in **Figure 8c**) the discharge rate of the inner pipe exceeds that of the outer pipe. This ascertains that the collapse of the outer pipe is rapidly transferred to the inner pipe and is then followed by the longitudinal propagation of the buckle in both carrier and inner pipes. The rate of discharge in the carrier pipe and inner pipe gradually decays as time lapses, which is due to the introduction of the end-caps in the buckle zone.

The hyperbaric chamber propagation buckling results of the 80 × 2 mm carrier pipe and the PIP-1 system are shown in **Figure 9**. A small dent was imposed to the carrier pipe in the single-pipe test, which explains the lower buckle initiation pressure of the carrier pipe compared to that of PIP-2. As shown in **Figure 9b**, following the collapse of the carrier pipe the pressure inside the chamber drops drastically

(a)

(b)

(c)

Figure 10.
Buckle propagation response inside the hyperbaric chamber: (a) buckle propagation response of the PIP-3 (80 × 3 mm-40 × 1.6 mm) with dog-bone buckle shape, (b) buckle propagation response of PIP-3 with confined buckle shape and (c) buckle propagation response of PIP-3 showing interaction between dog-bone and confined buckle shape.

until the carrier pipe and inner pipe come into contact. Subsequently, a dog-bone buckle shape propagates along the PIP while the pressure is maintained at P_{p2}. Hyperbaric chamber tests of PIP-1 and PIP-2 were repeated twice each and no significant disparities were observed in the results.

Results of the PIP-3 with D_o/t_o = 26.7 from three hyperbaric chamber tests are depicted in **Figure 10**. Unlike the responses of PIP-1 and PIP-2, three distinctive modes of buckling were observed in PIP-3, namely: (1) the dog-bone buckle shape (flat-mode) shown in **Figure 10a**, (2) the confined buckle shape (U-mode) shown in **Figure 10b** and (3) a combination of dog-bone and U-shaped buckle shown in **Figure 10c**. The dog-bone mode of buckling is similar to the responses observed in PIPs with high D_o/t_o values (PIP-1 and PIP-2). In this mode of failure, PIP-3 remains straight after failure and a flat mode of buckling propagates through its length; however the deformed shape of the inner pipe is not symmetric in the cross-section (shown in **Figure 10a**). In the second hyperbaric chamber test of PIP-3 shown in **Figure 10b**, a confined buckle shape is observed. The confined buckle mode is propagated along the length of the PIP while the pressure in the chamber is escalated followed by rapid discharge of water from the outer and inner pipes. It is worth mentioning that this U-shape buckling mode was previously observed in confined-buckling tests of steel and aluminum tubes reported by [31, 32]. Stephan et al. [32] performed an experimental investigation on the collapse of 3 m long aluminum pipes, inserted inside a 2 m long confining steel pipe. They observed a flat mode (dog-bone buckle shape) in the unconfined section of the aluminum pipe and a U-mode buckle shape within the confined section. Their experiments showed that within the studied range (16 < D/t < 48), the confined buckle shape consistently propagated at higher pressure compared to the dog-bone buckle shape. However the comparison between **Figure 10a** and **Figure 10b** shows that in PIP-3, the U-shape buckling propagation (P_{p2} = 1820 kPa) is initiated at a slightly lower pressure than the propagation pressure of the dog-bone buckle shape (P_{p2} = 2044 kPa). In the third test, PIP-3 showed a dog-bone failure mode that had flipped into a U-mode shape. The average P_{p2} results from all the hyperbaric chamber tests are given in **Table 4**.

2.4 Finite element analysis on propagation buckling of pipe-in-pipe systems

Finite element simulation of 1.6 m long samples of PIPs used in the hyperbaric chamber tests were conducted using ANSYS 16.1 [20]. Thin 4-node shell elements (181) were used to model the carrier pipe and the inner pipe. The contact between the inner and outer pipes, and in between the inner surfaces of the inner pipe were modeled using non-linear frictionless contact and target elements (174 and 170).

| ID | Hyperbaric chamber | | Analytical | | FE |
	P_p (kPa)	P_{p2} (kPa)	$\frac{\hat{P}_{p2}}{P_{p2}}$	$\frac{\widetilde{P}_{p2}}{P_{p2}}$	$\frac{P_{p2}^{FE}}{P_{p2}}$
PIP-1	700	780	0.78	0.86	1.28
PIP-2	900	1620	0.59	0.69	0.86
PIP-3	1400	2020[*]	0.64	0.66	0.96

[*]*Corresponds to dog-bone buckle shape shown in Figure 2.5a.*

Table 4.
Comparison between hyperbaric chamber, analytical and FE results.

Symmetry is used and only one half of the pipeline is modeled. The mesh uses shell elements with seven integration points along the wall-thickness. To better facilitate the nonlinear analysis, a small ovalization ratio Ω (Eq. (9)) equal to 0.5% was introduced at mid-length on the carrier pipe in the FE model.

The nodes at either end of the PIPs were restrained from translation in all directions. A von Mises elastoplastic (bi-linear) material definition with isotropic hardening was adopted. The modulus of elasticity (E) and tangent modulus ($E/$) used in the FE models are also shown in **Table 3** and are based on the stress-strain curves obtained from the tensile longitudinal coupons taken from the pipe wall shown in **Figure 11a**. The yield stresses used in the FE models based on the stress-strain curves and are presented in **Table 3** as σ_{Yo} and σ_{Yi} for the outer pipe and inner pipe respectively. The FE predictions of the propagation pressure of PIP-2 and PIP-3 depicted in **Table 4** represent 86 and 96%, respectively, of the experimental results. However the propagation pressure obtained from the FE analysis overestimates the experimental results for PIP-1.

The pressure response and the deformed shape of PIP-1 from the FE analyses are shown in **Figure 11b**. The pressure is plotted against the normalized ovalization of the carrier and inner pipes ($\Delta D/D$). By increasing the hydrostatic pressure, the carrier pipe of PIP-1 in **Figure 11b** gradually deforms from the intact shape (I) into a deformed shape (II). At this stage the outer and inner pipes come into contact and a small deformation is observed in the inner pipe. The local collapse in the inner pipe is arrested which is followed by a slight increase in the pressure. The collapse is then propagated in the outer pipe until detained by the end-caps as depicted in the deformed shape (III). While the buckle approaches the endcaps, a higher pressure is required to maintain the volume inside the hyperbaric chamber. This increase, however, causes the inner pipe to collapse (IV). This mode of buckling in which the collapse propagates over the inner pipe was reported in [10, 12] to occur in a PIP system where the inner pipe is stiffer (has larger thickness and yield stress) than the outer pipe. However we observed this buckling mode in PIP-1, in which the inner pipe is softer than the outer pipe.

2.5 Empirical expressions for propagation buckling of PIPs with thin and moderately thin carrier pipes

A comprehensive parametric study is conducted using the validated FE model to find the buckle propagation pressures of PIP systems with various wall thickness t_i/t_o, diameter D_i/D_o, and the material yield stress σ_{Yi}/σ_{Yo} ratios. Prior to reviewing results of the parametric dependency of propagation buckling of PIPs, it is worth discussing the buckling modes observed in the FE simulations. The FE analyses showed two dominant modes of failure under external pressure in the studied PIPs. In a thin PIP (D_o/t_o of 40) shown in **Figure 12**, and with a thick ness ratio of t_i/t_o = 0.6 and identical outer and inner pipes, mode A is observed. In mode A, by increasing the external pressure, the carrier pipe collapses and gradually deforms from the undeformed shape (I) into the deformed shape (II). Then, the outer and inner pipes touch. The touchdown point corresponds to (II) in **Figure 12**. Then, the pressure needs to get larger so that the collapse propagates along both outer and inner pipes shown in stages (III) to (IV).

Figure 13 shows the pressure response and the deformed shape of a moderately thin PIP with D_o/t_o of 30 and t_i/t_o of 0.8. The outer and inner pipes are identical. Following the initiation of collapse in the outer pipe, the pressure in the system is dropped and the buckle is propagated in the carrier pipe as shown in deformed shapes of II and III in **Figure 13**. At (III) the collapse has reached the end caps, therefore, a higher pressure is required to perpetuate the collapse in the outer pipe. However the increase in pressure causes a collapse in the inner pipe at the pressure

(a)

(b)
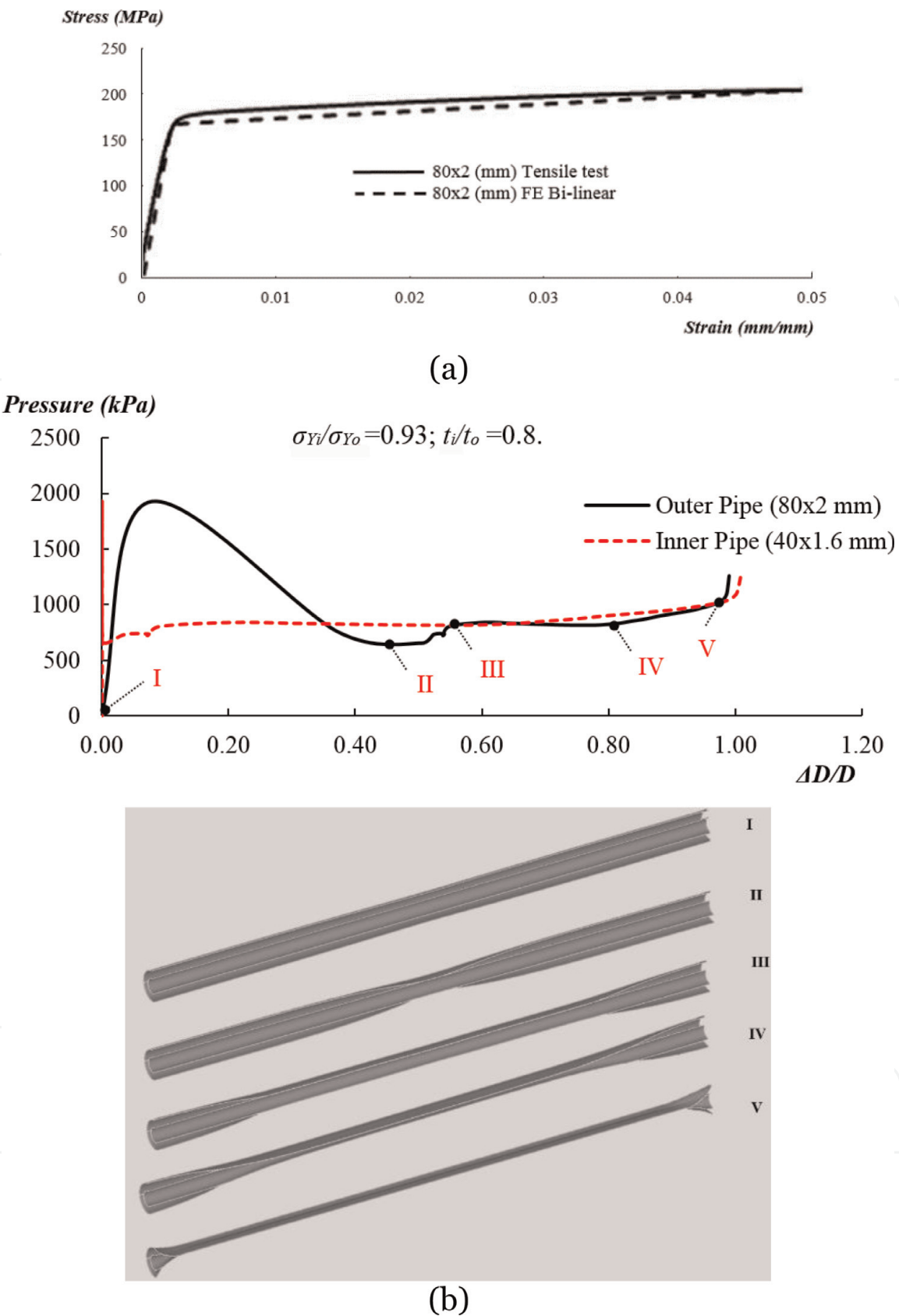
Figure 11.
(a) Experimental and FE stress–strain curves; (b) FE results showing pressure against normalized ovality and corresponding PIP-1 deformed shapes.

level (IV) and initiates a buckle which is propagated through the length (V). This buckle propagation mode is referred to as mode *B* in this study.

The parametric study ascertained the dependency of the propagation pressure of the PIP systems on geometric and material parameters of the outer and inner pipes. Moreover, current FE results proved that the buckle propagation modes of PIPs with large D_o/t_o ratios are not essentially similar to mode *A* predicted in previous
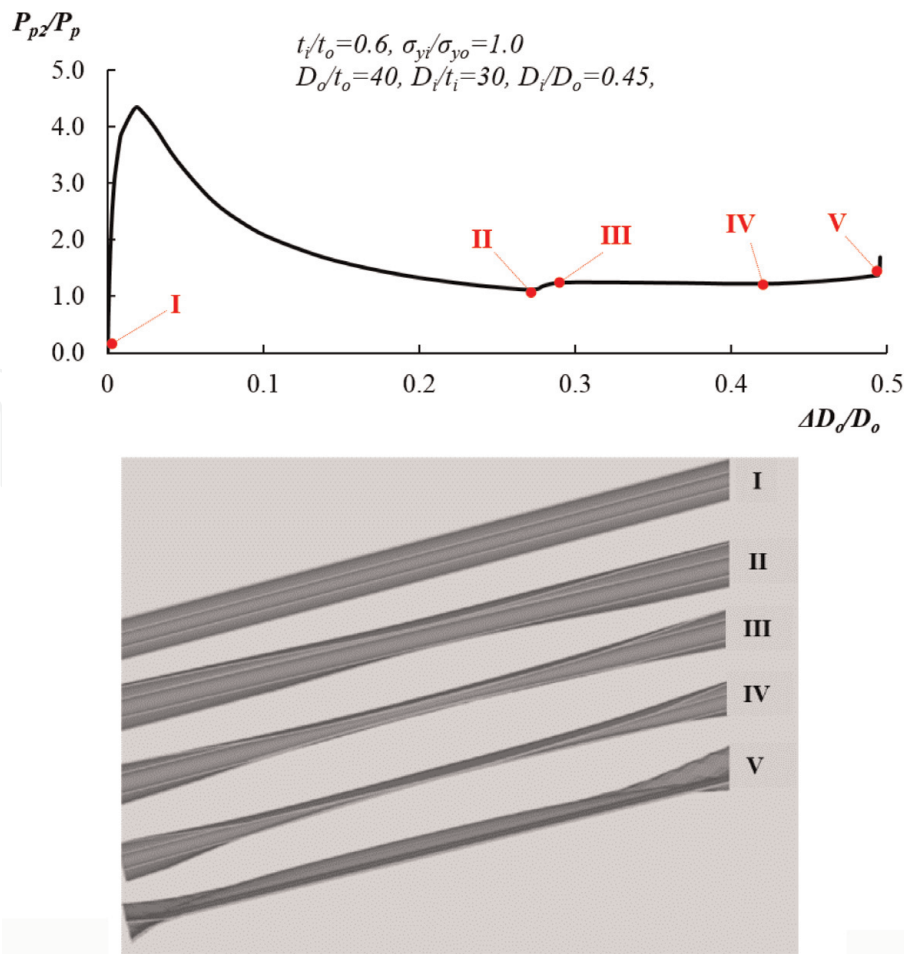
Figure 12.
Finite element results showing pressure against normalized ovality and corresponding deformed shapes of PIP system exhibiting buckle propagation mode A.

studies [11, 12]. Since proposed equations in the previous studies [11, 12] are incapable of predicting proper estimates of propagation pressure of PIPs that exhibit buckle propagation mode *B*, it is sensible to propose expressions for buckle propagation modes *A* and *B* separately. Based on a non-linear square fits of all the FE data points, the following empirical expressions can be suggested for Modes *A* and *B*.

$$\frac{P_{p2}}{P_p} = 1 + 1.047 \left(\frac{\sigma_{yi}}{\sigma_{yo}}\right)^{0.2} \left(\frac{D_i}{D_o}\right)^{0.4} \left(\frac{t_i}{t_o}\right)^{2.4} \tag{17}$$

$$\frac{P_{p2}}{P_p} = 1 + 0.596 \left(\frac{\sigma_{yi}}{\sigma_{yo}}\right)^{0.2} \left(\frac{D_i}{D_o}\right)^{-0.8} \left(\frac{t_i}{t_o}\right)^{2.4} \tag{18}$$

The coefficients in Eqs. (17) and (18) are determined using the Leven-berg-Marquardt algorithm and correspond to correlation factors (R^2) of 0.9827 and 0.9860 respectively. Comparison between the FE results and the proposed expressions are shown in **Figures 14a,b** for buckle propagation modes *A* and *B* respectively. The maximum differences between FE results and empirical expressions are less than 6.0%.

2.6 Empirical expressions for propagation buckling of PIPs with thick and moderately thick carrier pipes

In PIP systems with thin and moderately thin carrier pipes, expressions (Eqs. (17) and (18)) derived in Section 2.5 can be used to predict the propagation
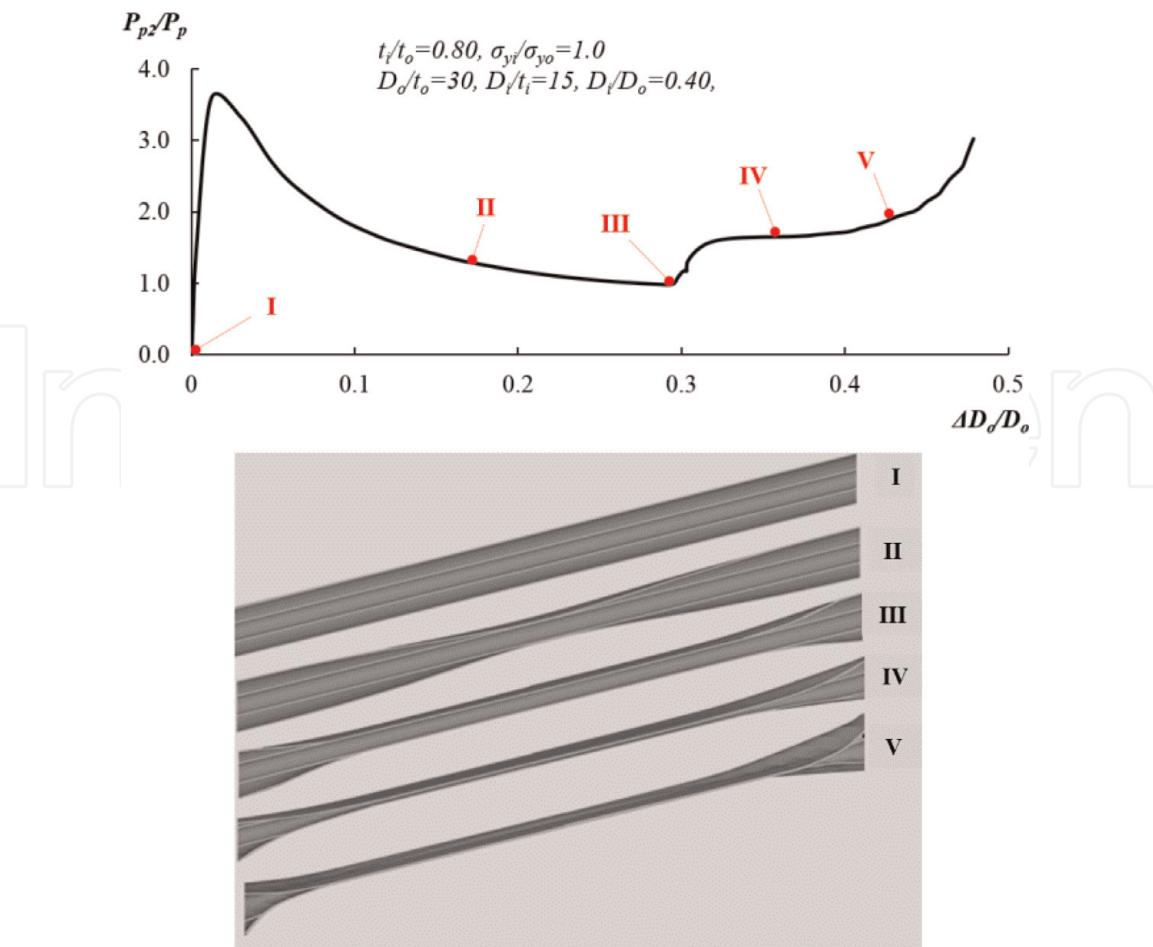
Figure 13.
Finite element results showing pressure against normalized ovality and corresponding deformed shapes of PIP system exhibiting buckle propagation mode B.

pressures. A total of 254 data points were collected from the raw data reported in [11, 12], and the current FE results for PIPs with D_o/t_o = 26.67. These data were used to propose an expression to predict the propagation pressure of PIPs with thick and moderately thick carrier pipes. Using the Levenberg-Marquardt algorithm of non-linear least squares the following expression was derived for the propagation pressure, P_{p2}, of PIPs with $D_o/t_o < 27$.

$$\frac{P_{p2}}{P_p} = 1 + 0.803 \left(\frac{\sigma_{yi}}{\sigma_{yo}}\right)^{0.4} \left(\frac{D_i}{D_o}\right)^{0.13} \left(\frac{t_i}{t_o}\right)^{1.8} \qquad (19)$$

with multiple correlation factor (R^2) of the fit is 0.9781. Similar procedure is used to derive (Eq. (19)). The expression accounts for the interaction between non-dimensional variables. For sake of brevity, the procedure is not shown here. Finally, the current FE results, the FE results of [12] and experimental results of [11] are collated in **Figure 15**, and are plotted against the proposed expression (Eq. (19)). The plot forms a nice linear band. The results in **Figure 15** correspond to buckle propagation mode *A*.

2.7 Empirical expression for collapse pressure Pci of PIPs

The hyperbaric chamber results disused in the previous section suggest that, the collapse pressure of the inner pipe of the PIP system, (P_{ci}), is a function of geometric and material parameters of both inner and outer pipes. A comprehensive parametric study carried out herein ascertained the dependency of the collapse pressure

(a)

(b)
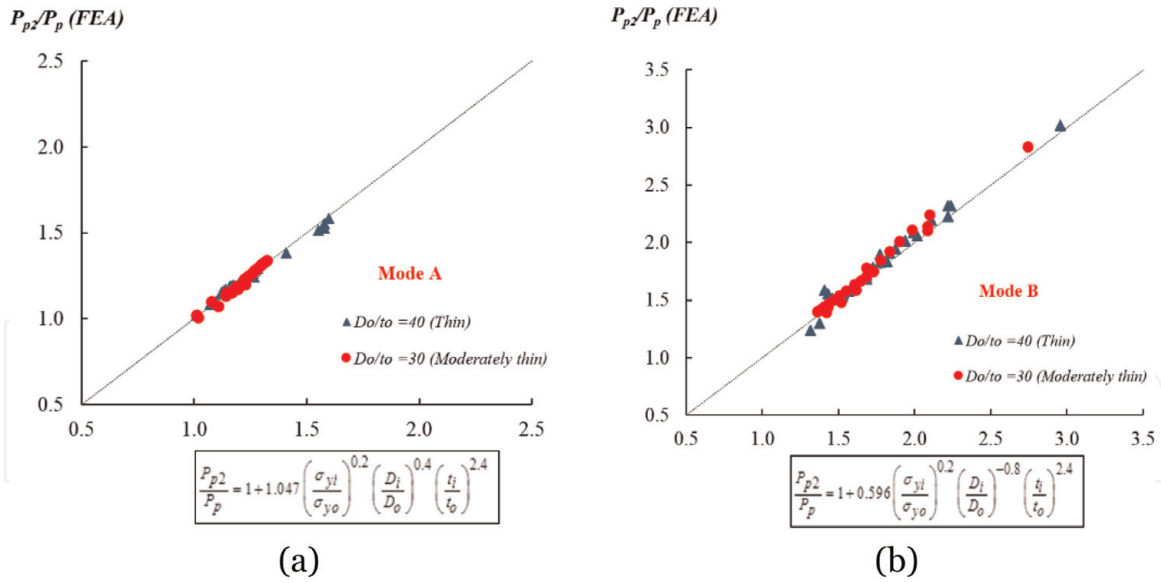
Figure 14.
Comparison between FE results and those predicted by Eqs. (17) and (18) of buckle propagation pressures of PIP with buckle propagation (a) mode A; and (b) mode B.
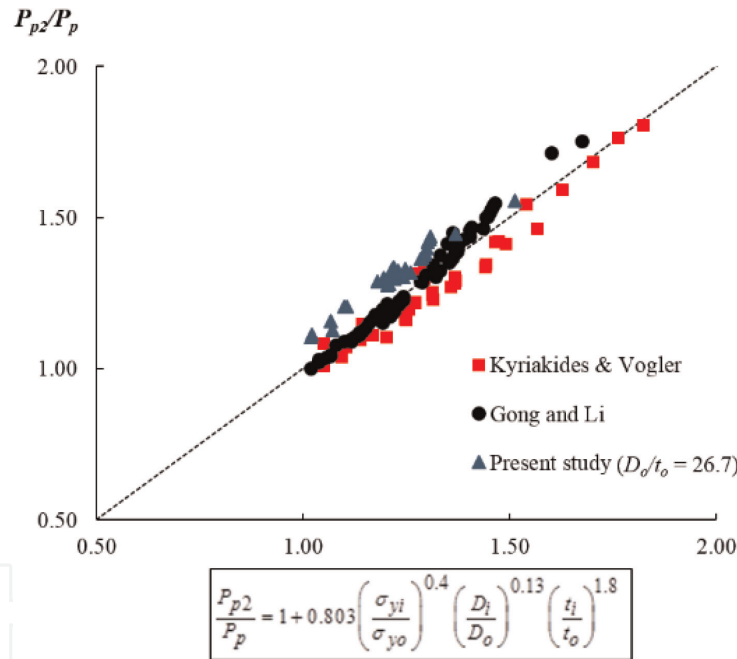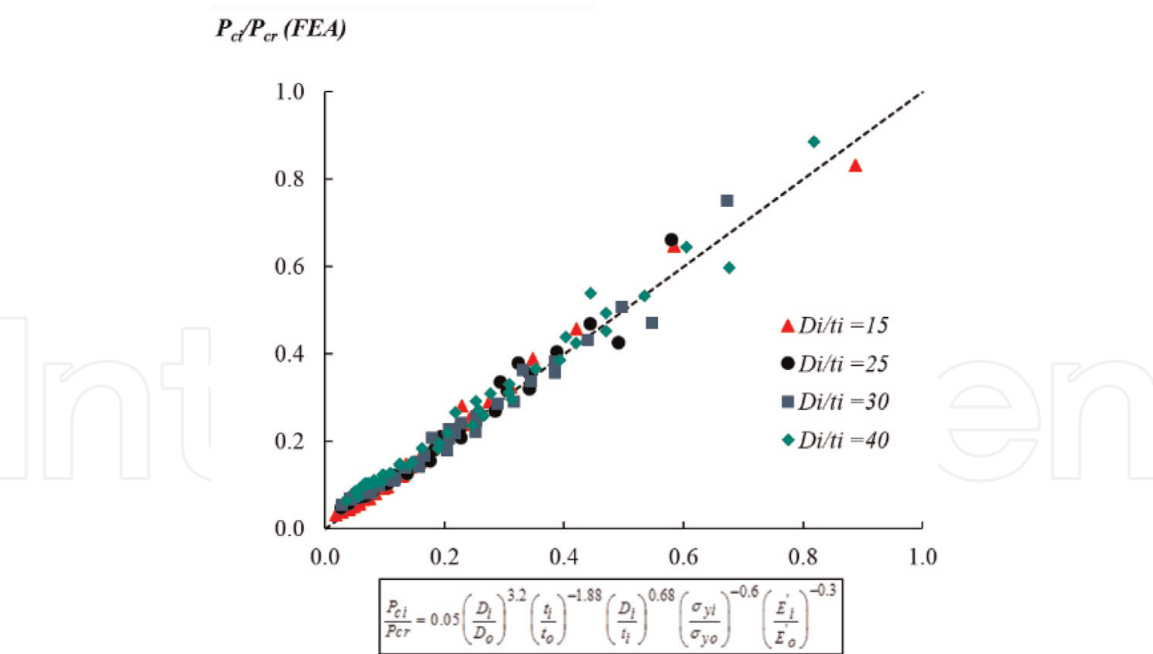

Figure 15.
Comparison between buckle propagation pressures of thick to moderately thick PIP systems from previous studies and current expression (all results correspond to the buckle propagation mode A).

P_{ci} of the PIP systems on geometric and material parameters of the outer and inner pipes. Based on the results of the parametric study and using non-linear square fits of sets of data taken from the FE results, the following normalized expression is derived for the collapse pressure of the inner pipe of PIPs.

$$\frac{P_{ci}}{Pcr} = 0.05 \left(\frac{D_i}{D_o}\right)^{3.2} \left(\frac{t_i}{t_o}\right)^{-1.88} \left(\frac{D_i}{t_i}\right)^{0.68} \left(\frac{\sigma_{yi}}{\sigma_{yo}}\right)^{-0.6} \left(\frac{E'_i}{E'_o}\right)^{-0.3} \tag{20}$$

The coefficient (0.05) in Eq. (20) is determined using the Levenberg-Marquardt algorithm with a correlation factor (R^2) of 0.9882. Comparison between the FE results and the proposed expression (Eq. (20)) is depicted in **Figure 16** for the

Figure 16.
Comparison between FE results and those predicted by Eq. (20).

	P_{ci}/P_{cr} (Eq. (20))	P_{ci}/P_{cr} (Exp.)	Difference (%)
PIP-1	0.173	0.166	4.05
PIP-2	0.077	0.077	0.00
PIP-3	0.188	0.184	2.13

Table 5.
Comparison between empirical and experimental collapse pressures.

studied range of D_i/t_i. The maximum difference between FE results and empirical expression (Eq. (20)) is less than 6.0%.

The normalized collapse pressures obtained from the proposed empirical expression (Eq. (20)) and those acquired from the hyperbaric chamber for the tested PIPs are represented in **Table 5**. The differences are less than 5%. As represented in the last column of **Table 5**, the empirical expression predicts the experimental results with good accuracy.

3. Conclusion

Buckling propagation mechanisms of subsea single-walled pipelines and pipe-in-pipe (PIP) systems under external pressure in quasi-static steady-state conditions were investigated using 2D analytical solutions, hyperbaric chamber and 3D FE analyses considering non-linear material and geometric behavior. In general, reasonable agreement is obtained between analytical, numerical and experimental results. The modified analytical solution suggested in this chapter accounts for the D_i/D_o ratio and provides more accurate predictions of the propagation buckling pressure of PIPs compared to the previous analytical equations. Confined buckling and flip-flop buckling modes were discovered in the hyperbaric chamber test of PIP-3 9 (**Table 3**). Nonlinear finite element analyses were conducted and verified against the hyperbaric chamber tests. The FE models provided valuable information about the buckling modes and progress in the carrier and inner pipes.

The comprehensive FE study suggested the existence of two major buckle modes in PIPs with thin and moderately thin carrier pipes. In mode *A* the buckle propagated simultaneously in the outer and inner tubes and in mode *B* the buckle propagated in the outer pipe and the collapse in the inner pipe was delayed. For each buckling mode, a separate expression was proposed, (Eqs. (17) and (18)). Based on the combined data from previous studies and current FE results, a more accurate empirical expression (Eq. (19)) was proposed to predict the propagation pressure P_{p2} of PIPs with thick and moderately thick carrier pipes. Moreover, the collapse pressure of the inner pipe of the PIP (P_{ci}) system was formulized. The proposed expression was shown to be in good agreement with hyperbaric chamber test results.

Author details

Hassan Karampour* and Mahmoud Alrsai
Griffith School of Engineering and Built Environment, Griffith University, QLD, Australia

*Address all correspondence to: karampour@griffith.edu.au

IntechOpen

References

[1] Kyriakides S, Corona E. Mechanics of Offshore Pipelines: Volume 1 Buckling and Collapse. Vol. 1. Oxford, UK: Elsevier; 2007

[2] Albermani F, Khalilpasha H, Karampour H. Propagation buckling in deep sub-sea pipelines. Engineering Structures. 2011;**33**(9):2547-2553

[3] Mesloh RE, Sorenson JE, Atterbury TJ. Buckling and offshore pipelines. Gas. 1973;**49**(7):40-43

[4] Palmer AC, Martin JH. Buckle propagation in submarine pipelines. Nature. 1975;**254**(5495):46

[5] Kyriakides S, Babcock CD. Experimental determination of the propagation pressure of circular pipes. Journal of Pressure Vessel Technology. 1981;**103**(4):328-336

[6] Kyriakides S, Netto TA. On the dynamics of propagating buckles in pipelines. International Journal of Solids and Structures. 2000;**37**:6843-6867

[7] Kamalarasa S, Calladine CR. Buckle propagation in submarine pipelines. International Journal of Mechanical Sciences. 1988;**30**(3–4):217-228

[8] Palmer AC, King RA. Subsea pipeline engineering. Oklahoma, USA: PennWell Books; 2004

[9] Xue J, Fatt MH. Buckling of a non-uniform, long cylindrical shell subjected to external hydrostatic pressure. Engineering Structures. 2002;**24**(8):1027-1034

[10] Kyriakides S. Buckle propagation in pipe-in-pipe systems: Part I. Experiments. International Journal of Solids and Structures. 2002;**39**(2):351-366

[11] Kyriakides S, Vogler TJ. Buckle propagation in pipe-in-pipe systems: Part II. Analysis. International Journal of Solids and Structures. 2002;**39**(2):367-392

[12] Gong S, Li G. Buckle propagation of pipe-in-pipe systems under external pressure. Engineering Structures. 2015;**84**:207-222

[13] Karampour H, Alrsai M, Albermani F, Guan H, Jeng DS. Propagation buckling in subsea pipe-in-pipe systems. Journal of Engineering Mechanics. 2017;**143**(9):04017113

[14] Alrsai M, Karampour H, Albermani F. Numerical study and parametric analysis of the propagation buckling behaviour of subsea pipe-in-pipe systems. Thin-Walled Structures. 2018;**125**:119-128

[15] Estefen SF, Netto TA, Pasqualino IP. Strength analyses of sandwich pipes for ultra deepwaters. Journal of Applied Mechanics. 2005;**72**(4):599-608

[16] Showkati H, Shahandeh R. Experiments on the buckling behavior of ring-stiffened pipelines under hydrostatic pressure. Journal of Engineering Mechanics. 2009;**136**(4):464-471

[17] Timoshenko SP, Gere JM. Theory of Elastic Stability. NewYork, USA: McGraw-Hill; 1961

[18] Kyriakides S, Babcock CD. On the dynamics and the arrest of the propagating buckle in offshore pipelines. In: Offshore Technology Conference. 1979;(1):45-57

[19] Mesloh R, Johns TG, Sorenson JE. The propagating buckle. Boss. Proceedings. 1976;**76**:787–797

[20] ANSYS 16.1 Release, A. I. 275 Technology Drive, Canonsburg, PA 15317

[21] Bai Y, Bai Q, editors. Subsea Pipelines and Risers. Oxford, UK: Elsevier; 2005

[22] Jukes P, Eltaher A, Sun J, Harrison G. Extra high-pressure high-temperature (XHPHT) flowlines: Design considerations and challenges. In: Proceedings of the ASME 2009 28th International Conference on Ocean, Offshore and Arctic Engineering. American Society of Mechanical Engineers. 2009. pp. 469-478

[23] Wang Z, Chen Z, Liu H. Numerical study on upheaval buckling of pipe-in-pipe systems with full contact imperfections. Engineering Structures. 2015;**99**:264-271

[24] Vaz MA, Patel MH. Lateral buckling of bundled pipe systems. Marine Structures. 1999;**12**(1):21-40

[25] Karampour H, Albermani F. Experimental and numerical investigations of buckle interaction in subsea pipelines. Engineering Structures. 2014;**66**:81-88

[26] Karampour H, Albermani F. Buckle interaction in textured deep subsea pipelines. Ships and Offshore Structures. 2016;**11**(6):625-635

[27] Karampour H, Albermani F, Gross J. On lateral and upheaval buckling of subsea pipelines. Engineering Structures. 2013;**52**:317-330

[28] Karampour H, Albermani F, Major P. Interaction between lateral buckling and propagation buckling in textured deep subsea pipelines. In: Proceedings of the ASME 34th International Conference on Ocean, Offshore and Arctic Engineering. American Society of Mechanical Engineers; 2015. pp. V003T02A079-V003T02A079

[29] Karampour H, Albermani F, Veidt M. Buckle interaction in deep subsea pipelines. Thin-Walled Structures. 2013;**72**:113-120

[30] Zheng J, Palmer A, Brunning P, Gan CT. Indentation and external pressure on subsea single wall pipe and pipe-in-pipe. Ocean Engineering. 2014;**83**: 125-132

[31] Lee LH, Kyriakides S. On the arresting efficiency of slip-on buckle arrestors for offshore pipelines. International Journal of Mechanical Sciences. 2004;**46**(7):1035-1055

[32] Stephan P, Love C, Albermani F, Karampour H. Experimental study on confined buckle propagation. Advanced Steel Construction. 2016;**12**(1):44-54

[33] Alrsai M, Karampour H, Albermani F. On collapse of the inner pipe of a pipe-in-pipe system under external pressure. Engineering Structures. 2018;**172**:614-628